

# Optically Addressable Molecular Spins at 2D Surfaces

Xuankai Zhou,<sup>1\*</sup> Yan-Tung Kong,<sup>1\*</sup> Cheuk Kit Cheung,<sup>1\*</sup> Guodong Bian,<sup>2,4</sup>  
Reda Moukaouine,<sup>2,5</sup> King Cho Wong,<sup>1</sup> Yumeng Sun,<sup>1</sup> Cheng-I Ho,<sup>1</sup>  
Vladislav Bushmakin,<sup>1</sup> Nils Gross,<sup>3</sup> Chun-Chieh Yen,<sup>3</sup> Tim Priessnitz,<sup>3</sup>  
Malik Lenger,<sup>1</sup> Sreehari Jayaram,<sup>1</sup> Takashi Taniguchi,<sup>8</sup> Kenji Watanabe,<sup>9</sup>  
Anton Pershin,<sup>2,6</sup> Ruoming Peng,<sup>1†</sup> Ádám Gali,<sup>2,6,7</sup> Jurgen Smet,<sup>3</sup>  
Jörg Wrachtrup<sup>1,3</sup>

<sup>1</sup>3. Physikalisches Institut, University of Stuttgart, 70569 Stuttgart, Germany

<sup>2</sup>HUN-REN Wigner Research Centre for Physics, Institute for Solid State  
Physics and Optics, P.O. Box 49, H-1525, Budapest, Hungary

<sup>3</sup>Max Planck Institute for Solid State Research, 70569 Stuttgart, Germany

<sup>4</sup>School of Chemistry, University of Birmingham, B15 2TT, Edgbaston, Birmingham, UK

<sup>5</sup>György Hevesy Doctoral School, ELTE Eötvös Loránd University, Institute of Chemistry,  
H-1117 Budapest, Hungary

<sup>6</sup>Department of Atomic Physics, Institute of Physics, Budapest University of Technology  
and Economics, Műegyetem rakpart 3, 1111 Budapest, Hungary

<sup>7</sup>MTA-WFK Lendület “Momentum” Semiconductor Nanostructures Research Group,  
P.O. Box 49, H-1525, Budapest, Hungary

<sup>8</sup> Research Center for Materials Nanoarchitectonics, National Institute for Materials  
Science, 1-1 Namiki, Tsukuba 305-0044, Japan

<sup>9</sup> Research Center for Electronic and Optical Materials, National Institute for Materials  
Science, 1-1 Namiki, Tsukuba 305-0044, Japan

\*Equal contributions

†E-mail: ruoming.peng@pi3.uni-stuttgart.de

**Optically addressable spins at material surfaces have represented a long-standing ambition in quantum sensing, providing atomic resolution and quantum-limited sensitivity. However, they are constrained by a finite depth at which the quantum spins can be stabilized. Here, we demonstrate a hybrid molecular-2D architecture that realizes quantum spin sensors directly on top of the surface. By anchoring spin-active molecules onto hexagonal boron nitride (hBN), we eliminate the depth of the quantum sensor while also exhibiting robust spin properties from 4 K to room temperature (RT). The Hahn-echo spin coherence time exceeds  $T_2 = 3.4 \mu\text{s}$  at 4 K, outperforming values in bulk organic crystals and overturning the prevailing expectation that spin inevitably deteriorates upon approaching the surface. By chemically tuning the molecule through deuteration,  $T_2$  improves by more than 10-fold, and under dynamic decoupling, coherence is prolonged to the intrinsic lifetime limit, exceeding 300  $\mu\text{s}$ . Proximal proton spins and the magnetic response of two-dimensional magnets beneath the hBN layer have been detected at RT. These molecular spins form surface quantum sensors with long coherence, optical addressability, and interfacial versatility, enabling a scalable, adaptable architecture beyond what conventional solid-state platforms offer.**

## Introduction

Quantum sensing has emerged as a powerful technology for probing matter at the nanoscale (1). Applications range from single nuclear magnetic resonance detection to the direct imaging of emergent phases in quantum materials, such as magnetism and superconductivity (2, 3). By combining long-lived quantum coherence with nanometer spatial resolution, spin-based platforms provide unique opportunities to access the electromagnetic responses at the atomic scale

that remain out of reach for conventional probes (4–10). Advancing the capabilities of quantum sensing requires that spin sensors are positioned ever closer to the target, ideally directly at the surface itself (11). However, this longstanding pursuit has faced persistent difficulties: defects, adsorbates, and surface terminations introduce a variety of noise sources that significantly degrade the spin coherence, charge stability, and sensitivity, in particular when the spin-to-surface distance drops below 10 nm (12–14). Despite recent advances in bulk solid-state hosts like diamond and SiC (15–17), the fundamental trade-off between depth and spin properties remains, motivating the exploration of alternative platforms.

Two-dimensional (2D) layered materials offer intrinsic structural stability and atomically clean interfaces with minimal surface-induced charge traps and no dangling bonds (18) and are therefore considered promising candidates for quantum sensing at surfaces (19–21). Multiple optically addressable spin defects have been identified in 2D hexagonal Boron Nitride (hBN) (22–26). However, their spin properties are limited by the dense nuclear spin environment of hBN (27) and the defects are often either too dim for efficient optical readout or challenging to reproducibly create due to the unclear defect structures (20, 28). It also remains a subject under debate whether such spin defects can be stabilized at the hBN surface, i.e. in the top hBN layers (29). So far, it is observed that the spin properties of the defects in hBN also degrade significantly as they approach the surface to less than 10 nm (30).

In parallel, molecular spin systems have also been extensively explored for a variety of quantum applications (31–35). While these systems offer chemically tunable quantum properties (36), they typically suffer from limited stability. They must be dispersed in bulk organic host crystals, where their spin properties again start to degrade when thinned down to below 100 nm (34). This renders surface integration and nanoscale positioning impractical. Moreover, many of these molecular spin candidates are only accessible at cryogenic temperatures with resonant excitation (32, 33, 35). That greatly limits their potential for robust quantum ap-

plications.

In order to overcome these limitations and realize stable spin systems with well-preserved spin-optical properties at the surface, we combine aromatic spin molecules-more specifically, pentacene (Pc)-with the 2D material hBN to construct a hybrid surface spin platform as illustrated in Fig.1a. Although such molecules have been deposited on hBN for high-quality organic electronics (37–40), their potential for quantum information processing at surfaces has remained entirely unexplored. The hBN can serve multiple purposes for molecular quantum sensing: (1) It provides a chemically inert and structurally stable substrate that protects the spin molecules from environmental degradation; (2) Its wide bandgap suppresses charge transfer from the Pc molecules, thereby maintaining the spin-triplet state; and (3) The lattice of B–N bonds in hBN closely matches the atomic spacing of C–C bonds in aromatic molecules, promoting the self-assembly of molecular arrays on the hBN surface; (4) Finally, it hosts a variety of surface defects that interact with and couple to Pc. This modifies the Pc energy levels of coupled Pc and mitigates unwanted annihilation processes from surrounding molecules. Together, these properties make hBN an ideal platform for integrating aromatic molecular spins toward the realization of quantum sensing at surfaces with prolonged spin coherence and enhanced stability.

## Optically Addressable Surface Spins

Pc–hBN devices are prepared via standard drop-casting/dip-coating techniques (see Supplementary Section 2). Pc is first dissolved in an organic solvent (e.g., chlorobenzene or toluene) with a concentration of  $\sim$ 10 mg/L, and then deposited onto the hBN flake positioned adjacent to a metal stripline. Because of the close match between the C–C and B–N bond lengths, as well as the hexagonal bond configuration of the molecule’s aromatic rings and the hBN lattice, two molecular orientations are favored at the surface, as illustrated in Fig.1a: face-on and edge-on. In the face-on phase, densely packed molecules exhibit strong spin diffusion and triplet

annihilation, which quench spin triplet states. In contrast, edge-on  $\text{Pc}$ , stabilized by native or intentionally introduced defects in the hBN surface layer, forms more decoupled molecules with weaker intermolecular coupling. As illustrated in Fig.1a, these edge-on molecules with a height of only 1.45 nm can act as coherent surface spins. Interactions with the hBN surface defects can distort the molecular orbitals, such as the highest occupied molecular orbitals (HOMO) of the triplet spins (Fig.1b), and the photoluminescence (PL) spectrum shows features of isolated  $\text{Pc}$  molecules—an essential prerequisite for maintaining active triplet spin states (31, 34). Specifically, we observe a zero-phonon line near 580 nm and a phonon sideband that matches the intrinsic isolated molecular vibrational mode (Fig. 1c).

The left inset of Fig.1d summarizes the observed spin transitions and electronic structure of an isolated  $\text{Pc}$  molecule. It features a singlet ground state ( $S_0$ ) and a series of excited states, including a long-lived triplet manifold. Upon 532-nm laser excitation, the molecule is excited from the singlet ground state to an excited singlet state ( $S_1$ ). The excited population can subsequently relax back either radiatively to the ground state via fluorescence, or non-radiatively by intersystem crossing (ISC) to a metastable triplet state ( $T$ ) with high yield, as commonly observed in organic host matrices. Due to the strong zero-field splitting (ZFS) intrinsic to  $\text{Pc}$  molecules and the additional symmetry reduction induced by the attachment to the hBN surface, the triplet state degeneracy is lifted. This results in three distinct sublevels:  $|T_x\rangle$ ,  $|T_y\rangle$ , and  $|T_z\rangle$ .

Continuous-wave (cw) ODMR measurements performed under ambient conditions reveal clear resonance features when the microwave frequency matches the energy separation between the triplet sublevels (schematically illustrated in the right inset of Fig.1d). The  $\text{Pc}$  on plasma-treated or electron-irradiated hBN exhibits enhanced ZFS constants, with the  $|T_y\rangle \leftrightarrow |T_z\rangle$  and  $|T_y\rangle \leftrightarrow |T_x\rangle$  transitions observed at 1433 MHz and 917 MHz, respectively. Using a double-resonance technique, holding one microwave tone at 1433 MHz and sweeping the second, we

uncover an additional resonance near 2350 MHz, confirming access to all triplet sublevels (Fig.1d). Importantly, we observe a linewidth of approximately 5 MHz for the  $|T_y\rangle \leftrightarrow |T_z\rangle$  transition. This value approaches the proton-limited linewidth typically reported for Pc in organic hosts. The molecular spins also show remarkable photostability, enabling cw-ODMR measurements lasting for days under ambient conditions and no changes for months at 4 K, far exceeding the stability reported in typical thin-film molecular systems. As shown in Supplementary Section 3, the time trace of photon counts shows a fast decay time of 2 hours and a slow decay exceeding two days, whereas the cw-ODMR contrast remains visible over the whole measurement duration.

We also manipulated spin states of Pc on hBN by driving Rabi oscillations at the  $|T_y\rangle \leftrightarrow |T_z\rangle$  transition. At room temperature, coherent control was achieved with 7% maximum contrast (Supplementary Section 7). It is still limited by the background fluorescence from defective hBN and uncoupled molecules. Hahn-echo measurements delivered a  $T_2$  of 2.4  $\mu$ s at room temperature and 3.4  $\mu$ s at 4 K (Fig.1e), exceeding the previously reported values of Pc in p-terphenyl (31). Unlike Pc in organic crystals, where  $T_2$  collapses as thin-film thickness is below  $\sim 200$  nm (34), Pc on hBN exhibits exceptional spin coherence, surpassing bulk values. AFM maps reveal ultrathin Pc clusters with a minimum thickness of 3 nm (Supplementary Section 4), confirming stabilization of Pc spin states at the interface. These results have established hBN as an exceptional surface host for aromatic molecular spins, with  $T_2$  values surpassing those of all known hBN spin defects by more than an order of magnitude across a broad range of temperatures.

## Hybrid Molecule-2D Framework

We now turn our attention to the role of hBN surface conditions to stabilize the coherent surface spins. Samples with three different surface treatments were studied in order to identify a cor-

relation between the surface defect density and the occurrence of spots with optically detected magnetic resonance (ODMR): pristine hBN with no treatment, electron irradiated hBN samples, and O<sub>2</sub>-plasma treated samples. The hBN samples with heavy O<sub>2</sub>-plasma bombardment show a strong increase in the number of ODMR spots, whereas in electron-irradiated samples, only a few spots are observed. In pristine high-quality hBN, almost none can be detected (See Supplementary Section 2 for more details).

For Pc embedded in organic host matrices, zero-field axial and rhombic splitting parameters *D* and *E* typically take on values of about 1400 MHz and 50 MHz, respectively (34, 41). For Pc on hBN, *D* and *E* are significantly larger. We obtain values of 1891 MHz and 459 MHz at room temperature. Moreover, the triplet population distribution differs markedly from the triplet population in an organic host, where the  $|T_x\rangle$  state is predominantly occupied (34). We argue that these differences reflect the altered local environment and highlight the importance of hBN and its defects in anchoring the Pc molecules. Indeed, DFT calculations show that Pc molecules can establish chemical bonds with defects on the hBN surface, leading to larger zero-field splitting parameters *D* and *E* than in free Pc (see Supplementary Section 9). By screening a variety of defect sites and configurations, we identify an edge-on Pc arrangement at V<sub>B</sub> – V<sub>N</sub> divacancies as one of the most energetically favorable Pc–defect complexes (Fig.2a). In this configuration, the spin density is confined toward the hBN plane, increasing *D*, while the concomitant reduction of molecular symmetry enhances the transverse parameter *E*. Most of the surface defect candidates we considered can promote the upright orientation of Pc molecules, which is particularly efficient if the defects incorporate boron vacancies (see Supplementary Section 9 for a detailed discussion). This is consistent with previous experimental reports of edge-on Pc on defective hBN (39).

To determine the spin configuration of Pc, we performed vector-field mapping of the spin transitions. By applying magnetic fields along different orientations, the molecular axis can

be identified through a fitting of the field-dependent ODMR response. In Fig.2b, we present the ODMR spectrum as a function of the magnetic field applied along the z-direction, i.e., the direction perpendicular to the hBN layer. The  $|T_x\rangle \leftrightarrow |T_y\rangle$  and  $|T_y\rangle \leftrightarrow |T_z\rangle$  transitions shift in opposite directions. By combining the responses for the other two orthogonal field orientations (See Supplementary Section 6), we are able to unequivocally demonstrate that the observed ODMR spots originate from Pc molecules with edge-on orientations on the hBN flakes as schematically shown in Fig.1a. Raman spectra recorded at these ODMR-active spots were compared with Raman spectra acquired on the bare substrate area (Supplementary Section 5). The mode not observed on the bare substrate but near the ODMR active spot at  $1533\text{ cm}^{-1}$  is a clear Raman signature of the edge-on configuration (42), corroborating the previous ODMR assignment. Here, the ODMR contrast remains clearly resolved for the intermediate spin-triplet manifold even under a large magnetic field (see Supplementary Section 6) applied off the molecular quantization axis (molecular z axis). This enables vector-resolved magnetic sensing with a significantly expanded dynamic range, overcoming the limitations of standard NV magnetometry where ODMR contrast diminishes under large off-axis magnetic fields.

To understand how Pc interacts with hBN, we first determine its molecular orientation using a polarization-resolved measurement. Because the Pc optical transition dipole lies along the molecular y-axis, as illustrated in Fig.2a, its absorption is intrinsically linearly polarized in this direction (43). Using this property, we control the excitation polarization by rotating a half-wave plate. By measuring the resulting polarization-dependent fluorescence, we can reliably determine the molecular axis of Pc on hBN. Statistical data collected on over 100 spin-active sites reveal that the orientation of the molecules is clustered into three groups (Fig.2d), one aligned with the long boundary of the hBN flake, referred to as  $0^\circ$ , and the other near  $60^\circ$  and  $120^\circ$ , reflecting the threefold symmetry of the hBN lattice. These data are shown in Fig.2c together with three polarization maps representative of each group. In view of the three-fold symmetry

and since exfoliated hBN flakes frequently exhibit straight edges along one of their crystalline directions, the y-axis of the ODMR active molecules apparently aligns with the hBN bonds. This corroborates the scenario that such molecules interact strongly with the hBN, possibly via two adjacent defect sites  $V_B - V_N$  (although alternative configurations are also conceivable; see Supplementary Section 9), where this interaction drives self-oriented molecular assembly.

## Lifetime-Limited Coherence Towards Surface Sensing

Since the  $P_c$  stands upright on the hBN surface, it is spatially lifted from the plane of boron and nitrogen atoms. This effectively decouples from the nuclear spins of the hBN substrate, and the coherence is limited mainly by the protons in the molecule itself. Hence, the  $P_c$  experiences a much cleaner magnetic environment compared to an intrinsic defect in hBN (27), as well as  $P_c$  embedded in an organic host, where additional nuclear spins from the matrix contribute to the decoherence. This simplifies the system considerably, since other nuclear sources only contribute marginally. It also turns this configuration particularly suitable for investigating whether isotope engineering and dynamical decoupling (DD) sequences can mitigate remaining sources of decoherence to further enhance performance.

Since the gyromagnetic ratio of deuterium is 6.5 times smaller than that of hydrogen, we considered deuterated  $P_c$  ( $P_c\text{-D}_{14}$ ) to benefit from the reduced hyperfine coupling as illustrated in Fig.3a, and indeed, at 4 K, a coherence time  $T_2$  of 39.8  $\mu\text{s}$  is observed for the  $|T_y\rangle - |T_z\rangle$  manifold (Fig.3b). This is a more than 10-fold improvement over the  $T_2$  for  $P_c\text{-H}_{14}$ . The oscillations in the  $P_c\text{-D}_{14}$  Hahn-echo traces likely arise from quadrupolar coupling of deuterium or other nuclei associated with the substrate. We also implemented dynamical decoupling to suppress the impact of low frequency noise using the Carr–Purcell–Meiboom–Gill (CPMG) sequences. A systematic increase is observed when dynamical decoupling pulses are applied. In our spin-protection scheme shown in Fig.3c, the  $|T_x\rangle$  and  $|T_z\rangle$  states are long-lived triplet

sublevels for spin manipulation, whereas the  $|T_y\rangle$  state is short-lived and is used to perform the readout (See detailed characterizations of lifetime in Supplementary Section 7). In deuterated  $\text{Pc}$ , we have achieved a  $T_{2,DD}$  exceeding 300  $\mu\text{s}$  with this configuration (Fig.3d). Even more, both  $|T_y\rangle \leftrightarrow |T_z\rangle$  and  $|T_x\rangle \leftrightarrow |T_z\rangle$  transitions can reach the lifetime limitation of each spin manifold as summarized in Fig.3e (See detailed characterization in Supplementary Section 7). Dynamical decoupling also prolongs the coherence of normal  $\text{Pc}$  ( $\text{H}_{14}$ ) to  $T_{2,DD} \approx 130 \mu\text{s}$  as shown in Supplementary Section 7. These values represent record-long spin coherence times for hBN-related systems and are obtained despite being at the surface. These values are comparable to, or even surpass, those for implanted spin defects, generated in bulk crystals including diamond and SiC (44–46).

The robustness of their spin properties enables the  $\text{Pc}$  molecules to function as quantum sensors for detecting their surroundings. Here, we demonstrate that it's possible to use  $\text{Pc-H}_{14}$  to detect their own proton nuclear spins in a Hahn echo experiment at room temperature. In Fig.4a, we plot the time evolution of the ODMR photoluminescence signal for six different magnetic fields, reflecting degrees of electron spin polarization. The hyperfine interaction causes a periodic revival of the spin polarization with the periodicity determined by the Larmor frequency of the nuclei, and the decay unveils the coherence time. Fits to these Hahn-echo decays yield a gyromagnetic ratio of  $\sim 43 \text{ MHz/T}$  matching that of the protons in  $\text{Pc}$  (Fig.4b).

Finally, as proof of principle that these molecular sensors on hBN can be integrated into a device architecture for sensing 2D magnetic layer materials, we fabricated an hBN-encapsulated  $\text{Fe}_3\text{GaTe}_2$  (FGT) van der Waals heterostructure and deposited  $\text{Pc}$  molecules on the top hBN surface, as illustrated in Fig.4c. FGT has been recently identified as a room-temperature 2D ferromagnet (47). The hBN spacer defines the sensor–sample distance, allowing the molecular spins to detect magnetic responses from the underlying magnetic layer under ambient conditions (see more characterizations in Supplementary Section 8). Figure 4d illustrates that molecules

located near the FGT region exhibit clear ODMR shifts compared with those sitting on the bare substrate. The observed shift reflects a local magnetic response of roughly 1 mT. In this hybrid configuration, the ensemble of molecular spins operates as an integrated quantum sensor that uncovers the underlying magnetic behavior of the 2D magnet.

## Conclusions

In conclusion, we have demonstrated the operation of an optically addressable spin sensor directly at the interface by combining pentacene molecules with the 2D material hBN. The spin lifetime, spin coherence time, as well as the optical properties required for sensing, are preserved from 4 K up to room temperature. The spin coherence time not only surpasses that of molecular spin sensors embedded in an organic bulk matrix, but also exceeds those of all previously reported spin defects in hBN by more than an order of magnitude (22–26). Despite its position at the surface, this spin sensor reaches a coherence level comparable to that of many well-established spin defects that need to be buried inside the host material to avoid performance degradation. Particularly noteworthy is the excellent photostability of Pc spins at ODMR-active sites. The signals persist for days in ambient conditions under continuous laser illumination. This is not the case for organic molecules in a thin-film bulk matrix or solutions that suffer from severe photobleaching (48, 49). Apparently, the hBN host plays a stabilizing role, which may inspire new strategies for realizing other robust molecular sensors.

These hybrid sensors are inherently compatible with 2D-material fabrication and surface-NMR platforms, so that a seamless integration with a diverse set of device architectures is conceivable. By using wafer-scale hBN as a substrate, our molecular quantum system can be scaled to several inches with deterministic positioned molecules, opening new opportunities for quantum sensing. The device geometry, where the hBN covered with molecules is placed on top of the material to be studied, may benefit from a reduced hBN layer thickness in order to en-

hance the coupling strength of the spin sensor beyond the dipolar limit and enter the exchange-interaction regime (50). *Pc* represents only one example among many aromatic molecules that possess intermediate triplet states. A vast family of more than 10,000 related molecules exists with tunable chemical modifications (36, 51, 52), and hence the surface spin sensor concept put forward here can be extended to numerous other candidate molecules.

## Acknowledgments

We acknowledge funding support from the European Union through the project C-QuEnS (Grant No. 101135359); the BMBF through the projects QCOMP (Grant No. 03ZU1110HA), QSOLID (Grant No. 13N16159), and QMAT (Grant No. 03ZU2110HA); and the Zeiss Foundation through QPhoton. J.H.S. acknowledges support from the DFG Priority Program SPP 2244. A.G., A.P., G.B., and R.M. acknowledge support from the Quantum Information National Laboratory of Hungary, funded by the National Research, Development, and Innovation Office (NKFIH) under Grant No. 2022-2.1.1-NL-2022-00004. A.G. further acknowledges access to high-performance computational resources provided by KIFÜ (Governmental Agency for IT Development, Hungary), and funding from the European Commission through the QuSPARC (Grant No. 101186889) and SPINUS (Grant No. 101135699) projects. A.P. acknowledges the financial support of a János Bolyai Research Fellowship of the Hungarian Academy of Sciences. R.M. is grateful for support from the Stipendium Hungaricum scholarship.

## Author Contributions

R.P. and J.W. conceived the project. R.P., X.Z., and Y.K. fabricated Pc-hBN devices. X.Z., Y.K., C.C., and R.P. performed room-temperature characterization with assistance from K.W., Y.S., and C.H. X.Z., Y.K., C.C., and K.W. carried out cryogenic measurements, assisted by V.B., M.L., and S.J. C.Y. performed all AFM scans. N.G. and T.P. performed the Raman measurements. G.B., R.M., A.P., and A.G. performed the DFT analysis of molecule interactions. R.P. and J.H.S. wrote the paper, assisted by J.W., X.Z., Y.K., C.C., N.G., G.B., and A.G. R.P. supervised the research. All authors discussed the results and commented on the paper.

## References

1. C. L. Degen, F. Reinhard, P. Cappellaro, Quantum sensing, *Reviews of Modern Physics* **89**, 035002 (2017).
2. J. Du, F. Shi, X. Kong, F. Jelezko, J. Wrachtrup, Single-molecule scale magnetic resonance spectroscopy using quantum diamond sensors, *Reviews of Modern Physics* **96**, 025001 (2024).
3. F. Casola, T. van der Sar, A. Yacoby, Probing condensed matter physics with magnetometry based on nitrogen-vacancy centres in diamond, *Nature Reviews Materials* **3**, 17088 (2018).
4. G. Balasubramanian, *et al.*, Nanoscale imaging magnetometry with diamond spins under ambient conditions, *Nature* **455**, 648 (2008).
5. P. Maletinsky, *et al.*, A robust scanning diamond sensor for nanoscale imaging with single nitrogen-vacancy centres, *Nature Nanotechnology* **7**, 320 (2012).
6. T. Staudacher, *et al.*, Nuclear magnetic resonance spectroscopy on a (5-nanometer) 3 sample volume, *Science* **339**, 561 (2013).
7. L. Thiel, *et al.*, Probing magnetism in 2d materials at the nanoscale with single-spin microscopy, *Science* **364**, 973 (2019).
8. K. Bian, *et al.*, Nanoscale electric-field imaging based on a quantum sensor and its charge-state control under ambient condition, *Nature Communications* **12**, 2457 (2021).
9. T. Song, *et al.*, Direct visualization of magnetic domains and moiré magnetism in twisted 2d magnets, *Science* **374**, 1140 (2021).

10. M. L. Palm, *et al.*, Observation of current whirlpools in graphene at room temperature, *Science* **384**, 465 (2024).
11. R. Schirhagl, K. Chang, M. Loretz, C. L. Degen, Nitrogen-vacancy centers in diamond: Nanoscale sensors for physics and biology, *Annual Review of Physical Chemistry* **65**, 83 (2014).
12. Y. Romach, *et al.*, Spectroscopy of surface-induced noise using shallow spins in diamond, *Physical Review Letters* **114**, 017601 (2015).
13. D. Bluvstein, Z. Zhang, A. C. B. Jayich, Identifying and mitigating charge instabilities in shallow diamond nitrogen-vacancy centers, *Physical Review Letters* **122**, 076101 (2019).
14. S. Sangtawesin, *et al.*, Origins of diamond surface noise probed by correlating single-spin measurements with surface spectroscopy, *Physical Review X* **9**, 031052 (2019).
15. L. V. H. Rodgers, *et al.*, Materials challenges for quantum technologies based on color centers in diamond, *MRS Bulletin* **46**, 623 (2021).
16. G. Wolfowicz, *et al.*, Quantum guidelines for solid-state spin defects, *Nature Reviews Materials* **6**, 906 (2021).
17. P. Li, *et al.*, Non-invasive bioinert room-temperature quantum sensor from silicon carbide qubits, *Nature Materials* (2025).
18. C. R. Dean, *et al.*, Boron nitride substrates for high-quality graphene electronics, *Nature Nanotechnology* **5**, 722 (2010).
19. T. T. Tran, K. Bray, M. J. Ford, M. Toth, I. Aharonovich, Quantum emission from hexagonal boron nitride monolayers, *Nature Nanotechnology* **11**, 37 (2015).

20. S. Vaidya, X. Gao, S. Dikshit, I. Aharonovich, T. Li, Quantum sensing and imaging with spin defects in hexagonal boron nitride, *Advances in Physics: X* **8**, 2206049 (2023).
21. H.-H. Fang, X.-J. Wang, X. Marie, H.-B. Sun, Quantum sensing with optically accessible spin defects in van der waals layered materials, *Light: Science & Applications*, **13**, 303 (2024).
22. A. Gottscholl, *et al.*, Initialization and read-out of intrinsic spin defects in a van der waals crystal at room temperature, *Nature Materials* **19**, 540 (2020).
23. N. Mendelson, *et al.*, Identifying carbon as the source of visible single-photon emission from hexagonal boron nitride, *Nature Materials* **20**, 321 (2020).
24. N. Chejanovsky, *et al.*, Single-spin resonance in a van der waals embedded paramagnetic defect, *Nature Materials* **20**, 1079 (2021).
25. H. L. Stern, *et al.*, Room-temperature optically detected magnetic resonance of single defects in hexagonal boron nitride, *Nature Communications* **13**, 618 (2022).
26. X. Gao, *et al.*, Single nuclear spin detection and control in a van der waals material, *Nature* **643**, 943 (2025).
27. A. Haykal, *et al.*, Decoherence of  $V_{B^-}$  spin defects in monoisotopic hexagonal boron nitride, *Nature Communications* **13**, 4347 (2022).
28. W. Liu, *et al.*, Spin-active defects in hexagonal boron nitride, *Materials for Quantum Technology* **2**, 032002 (2022).
29. C. Dai, *et al.*, Evolution of nanopores in hexagonal boron nitride, *Communications Chemistry* **6**, 108 (2023).

30. A. Durand, *et al.*, Optically active spin defects in few-layer thick hexagonal boron nitride, *Physical Review Letters* **131**, 116902 (2023).
31. J. Wrachtrup, C. von Borczyskowski, J. Bernard, M. Orrit, R. Brown, Optical detection of magnetic resonance in a single molecule, *Nature* **363**, 244 (1993).
32. S. L. Bayliss, *et al.*, Optically addressable molecular spins for quantum information processing, *Science* **370**, 1309 (2020).
33. D. Serrano, *et al.*, Ultra-narrow optical linewidths in rare-earth molecular crystals, *Nature* **603**, 241 (2022).
34. A. Mena, *et al.*, Room-temperature optically detected coherent control of molecular spins, *Physical Review Letters* **133**, 120801 (2024).
35. L. R. Weiss, *et al.*, A high-resolution molecular spin-photon interface at telecommunication wavelengths, *Science* **390**, 76 (2025).
36. S. K. Mann, *et al.*, Chemically tuning room temperature pulsed optically detected magnetic resonance, *Journal of the American Chemical Society* **147**, 22911 (2025).
37. S. J. Kang, *et al.*, Organic field effect transistors based on graphene and hexagonal boron nitride heterostructures, *Advanced Functional Materials* **24**, 5157 (2014).
38. Y. Zhang, *et al.*, Probing carrier transport and structure-property relationship of highly ordered organic semiconductors at the two-dimensional limit, *Physical Review Letters* **116**, 016602 (2016).
39. D. Günder, K. Watanabe, T. Taniguchi, G. Witte, Van der waals bound organic/2d insulator hybrid structures: Epitaxial growth of acene films on hbn(001) and the influence of surface defects, *ACS Applied Materials & Interfaces* **12**, 38757 (2020).

40. S. H. Amsterdam, *et al.*, Tailoring the optical response of pentacene thin films via templated growth on hexagonal boron nitride, *The Journal of Physical Chemistry Letters* **12**, 26 (2020).

41. H. Singh, *et al.*, Room-temperature quantum sensing with photoexcited triplet electrons in organic crystals, *Physical Review Research* **7**, 013192 (2025).

42. K. Seto, Y. Furukawa, Study on solid structure of pentacene thin films using raman imaging, *Journal of Raman Spectroscopy* **43**, 2015 (2012).

43. A. Hinderhofer, *et al.*, Optical properties of pentacene and perfluoropentacene thin films, *The Journal of Chemical Physics* **127**, 194705 (2007).

44. B. Naydenov, *et al.*, Increasing the coherence time of single electron spins in diamond by high temperature annealing, *Applied Physics Letters* **97**, 242511 (2010).

45. C. Kasper, *et al.*, Influence of irradiation on defect spin coherence in silicon carbide, *Physical Review Applied* **13**, 044054 (2020).

46. W.-X. Lin, *et al.*, Temperature dependence of divacancy spin coherence in implanted silicon carbide, *Physical Review B* **104**, 125305 (2021).

47. G. Zhang, *et al.*, Above-room-temperature strong intrinsic ferromagnetism in 2D van der waals  $\text{Fe}_3\text{GaTe}_2$  with large perpendicular magnetic anisotropy, *Nature Communications* **13**, 5067 (2022).

48. J. Widengren, R. Rigler, Mechanisms of photobleaching investigated by fluorescence correlation spectroscopy, *Bioimaging* **4**, 149 (1996).

49. A. P. Demchenko, Photobleaching of organic fluorophores: quantitative characterization, mechanisms, protection, *Methods and Applications in Fluorescence* **8**, 022001 (2020).

50. S. Kovarik, *et al.*, Spin torque–driven electron paramagnetic resonance of a single spin in a pentacene molecule, *Science* **384**, 1368 (2024).
51. J. E. Anthony, D. L. Eaton, S. R. Parkin, A road map to stable, soluble, easily crystallized pentacene derivatives, *Organic Letters* **4**, 15 (2001).
52. H. Yamada, *et al.*, Photochemical synthesis of pentacene and its derivatives, *Chemistry – A European Journal* **11**, 6212 (2005).

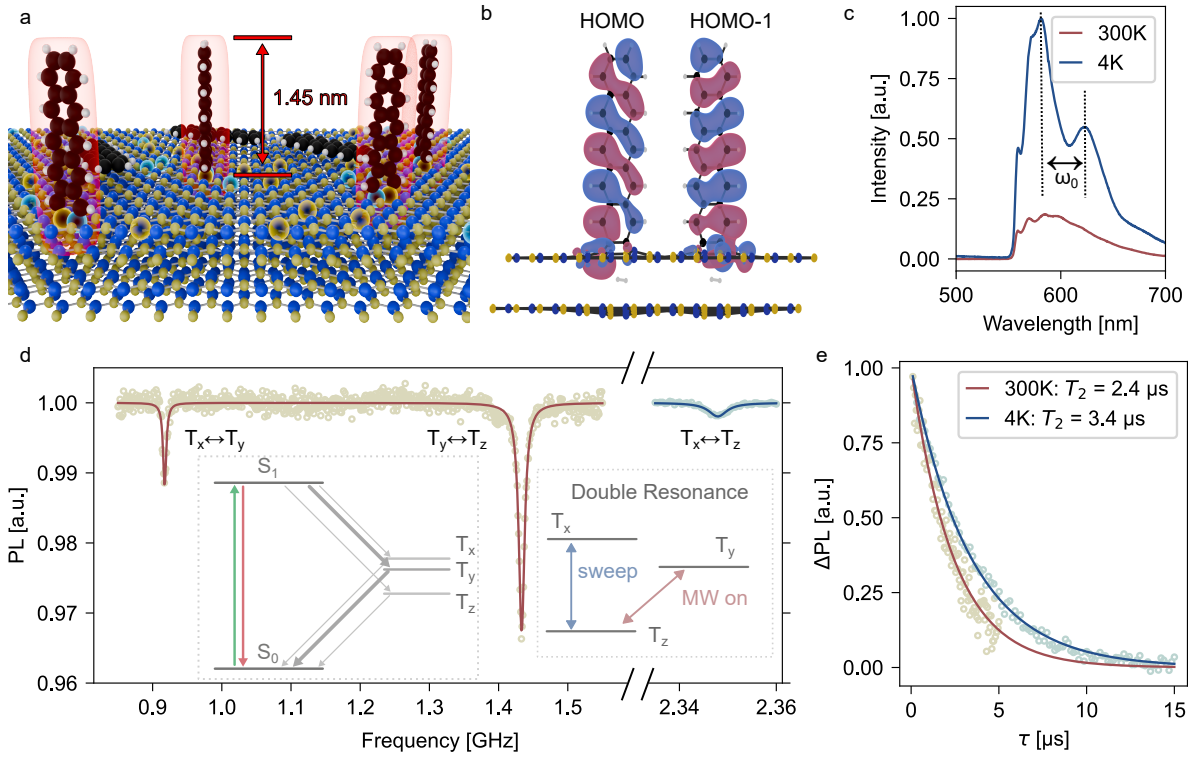


**Figure 1: Surface molecular spins hosted on hBN.** **a**, Schematic illustration of **Pc** molecules coupled to hBN surface defects in the edge-on configuration, which enables optical addressing of spins. **b**, Spatial distributions of the highest occupied molecular orbitals (HOMO) of the triplet spins. **c**, Photoluminescence spectra of **Pc** molecules on hBN at 4 K and room temperature.  $\omega_0$  denotes a characteristic molecular phonon mode. **d**, ODMR spectrum of **Pc** at ambient conditions, revealing the  $|T_x\rangle - |T_y\rangle$  and  $|T_y\rangle - |T_z\rangle$  transitions at 917 MHz and 1433 MHz, respectively. The  $|T_x\rangle - |T_z\rangle$  transition is accessed via a double-resonance scheme, as illustrated in the right inset, where two microwave tones are applied. **e**, Hahn-echo spin-coherence measurements of **Pc** spins at room temperature and 4 K, yielding a characteristic  $T_2$  time of 3.4  $\mu$ s at 4K.

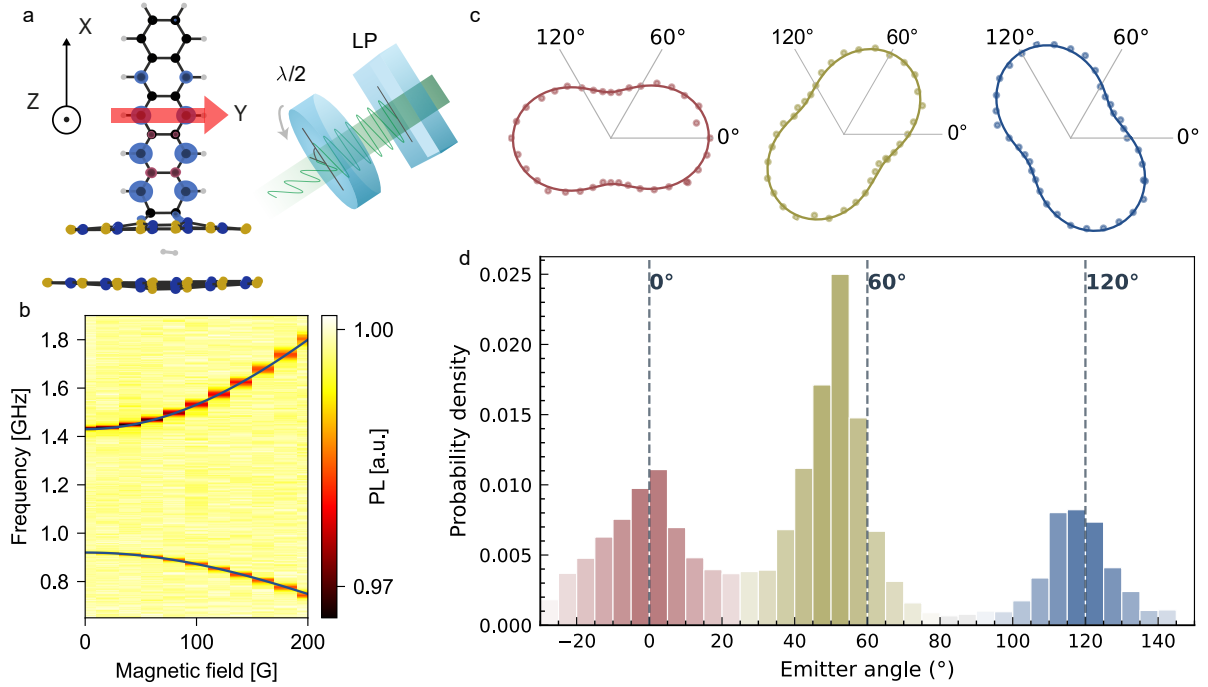


**Figure 2: Pc configuration on hBN surfaces.** **a**, Calculated spin-density distribution of Pc, showing a shift of spin density toward the hBN plane, which leads to an increased zero-field splitting with optical dipole orientation of the Pc aligned along the molecular Y axis. The molecular axis orientation is indicated according to the conventional definition. Right: schematic of the polarization-resolved measurement used to determine the Pc molecular Y-axis orientation. **b**, Out-of-plane Magnetic-field dependence of the  $|T_x\rangle - |T_y\rangle$  and  $|T_y\rangle - |T_z\rangle$  transitions, consistent with an edge-on configuration of Pc molecules. **c**, Representative polarization maps for Pc orientations at  $0^\circ$ ,  $60^\circ$ , and  $120^\circ$  with respect to the hBN edges show clear linear polarization behavior. **d**, Histogram of hundreds of Pc ODMR spots, revealing the threefold symmetry of Pc alignment relative to the underlying hBN lattice.

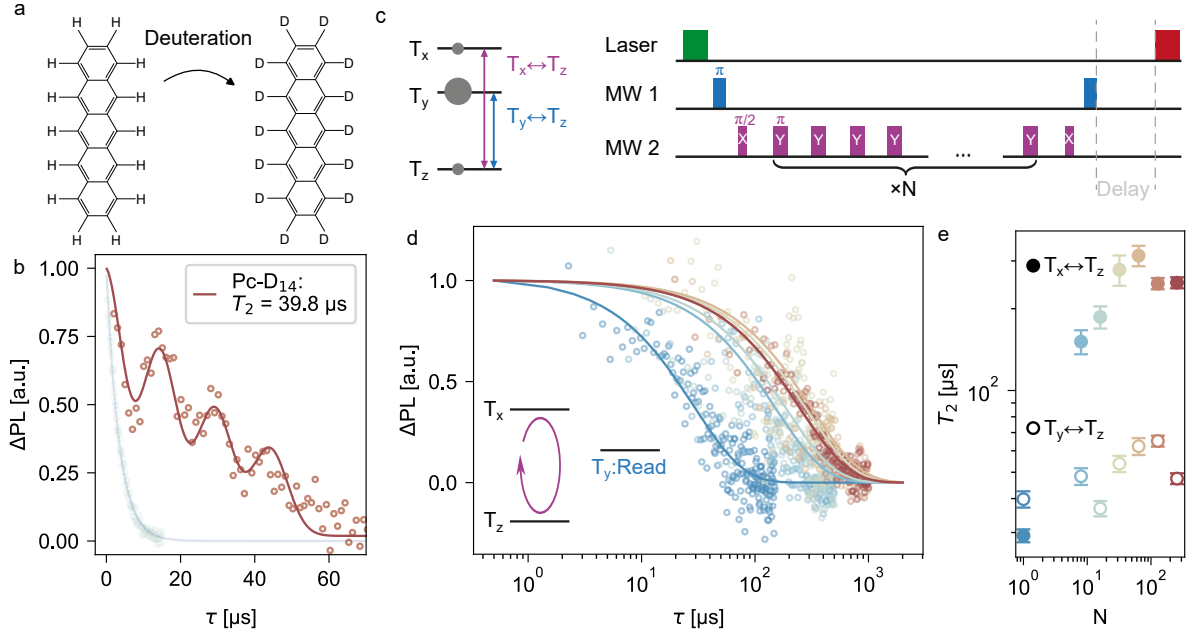


**Figure 3: Engineering of spin coherence toward the lifetime limit.** **a**, Schematic illustration of molecular deuteration from  $\text{Pc-H}_{14}$  to  $\text{Pc-D}_{14}$ , which suppresses nuclear-spin-induced decoherence. **b**, The Hahn-echo spin coherence time ( $T_2$ ) in  $\text{Pc-D}_{14}$  exhibits a tenfold enhancement relative to  $\text{Pc-H}_{14}$ . For comparison, the  $\text{Pc-H}_{14}$  data are plotted as a semi-transparent reference curve. **c**, Schematic of dynamical decoupling pulse sequences (CPMG) used to protect spin coherence in the molecular  $|\text{T}_x\rangle - |\text{T}_z\rangle$  basis with  $\text{T}_y$  for readout. **d**, Extended spin coherence of  $\text{Pc-D}_{14}$  under dynamical decoupling, with spins protected in the  $|\text{T}_x\rangle - |\text{T}_z\rangle$  manifold. **e**, The prolongation of the coherence time as a function of the number of applied  $\pi$  pulses  $N$ . For both the  $|\text{T}_y\rangle - |\text{T}_z\rangle$  and  $|\text{T}_x\rangle - |\text{T}_z\rangle$  transitions, the spin coherence approaches the lifetime limit for their own spin manifolds.

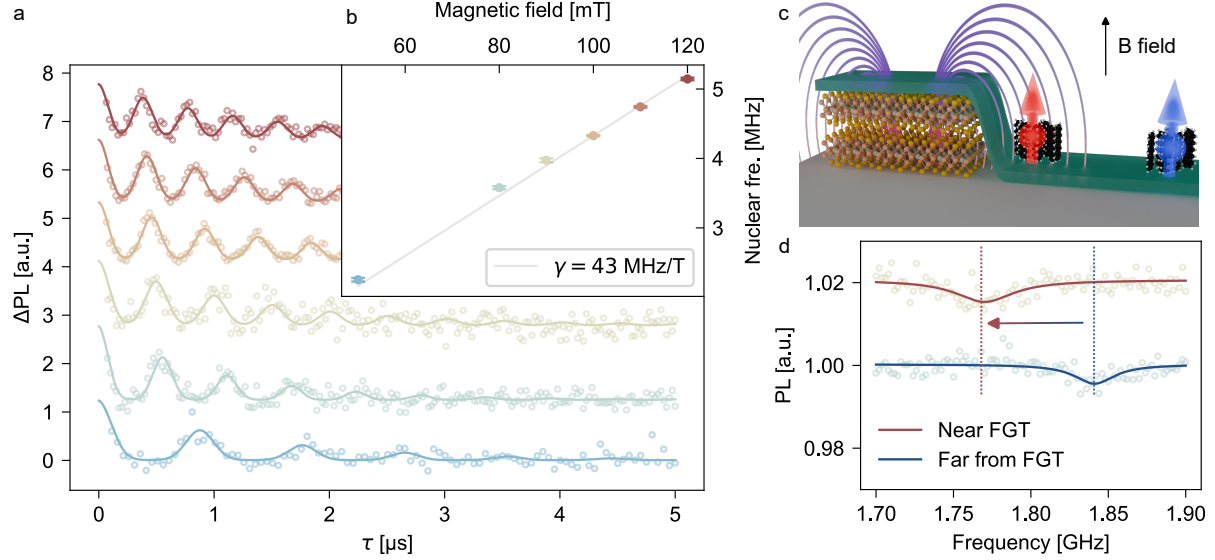


**Figure 4: Exploiting  $Pc$  as a room temperature spin surface sensor.** **a**, Hahn-echo measurements recorded for six different values of the magnetic field in order to detect  $Pc$ 's own proton spins.  $\Delta PL$  reflects the degree of spin polarization. The observed revivals in spin polarization indicate coupling to nearby nuclear spins. **b**, Field dependence of the nuclear precession frequency, showing an effective gyromagnetic ratio close to that of the protons. **c**, Illustration of the two-dimensional (2D) sensing architecture, where  $Pc$  molecules are deposited on an hBN layer that itself covers a 2D ferromagnet ( $Fe_3GaTe_2$ ). **d**, ODMR spectrum of  $Pc$  molecules located in the hBN area covering the 2D magnet. Also shown is a reference spectrum on hBN far away from FGT. The arrow marks the observed shift induced by the magnetic layer.